High throughput assembly of spatially controlled 3D cell clusters on a micro/nanoplatform†

Daniel Gallego-Perez,‡[a] Natalia Higuita-Castro,‡[a] Sadhana Sharma,‡[b] Rashmeet K. Reen,[a] Andre F. Palmer,[bc] Keith J. Gooch,[a] L. James Lee,[bc] John J. Lannutti[bd] and Derek J. Hansford*[ab]

Received 17th September 2009, Accepted 27th November 2009
First published as an Advance Article on the web 11th January 2010
DOI: 10.1039/b919475d

Guided assembly of microscale tissue subunits (*i.e.* 3D cell clusters/aggregates) has found applications in cell therapy/tissue engineering, cell and developmental biology, and drug discovery. As cluster size and geometry are known to influence cellular responses, the ability to spatially control cluster formation in a high throughput manner could be advantageous for many biomedical applications. In this work, a micro- and nanofabricated platform was developed for this purpose, consisting of a soft-lithographically fabricated array of through-thickness microwells structurally bonded to a sheet of electrospun fibers. The microwells and fibers were manufactured from several polymers of biomedical interest. Human hepatocytes were used as model cells to demonstrate the ability of the platform to allow controlled cluster formation. In addition, the ability of the device to support studies on semi-controlled heterotypic interactions was demonstrated by co-culturing hepatocytes and fibroblasts. Preliminary experiments with other cells of interest (pancreatic cells, embryonic stem cells, and cardiomyocytes) were also conducted. Our platform possesses several advantages over previously developed microwell arrays: a more *in vivo*-like topographical stimulation of cells; better nutrient/waste exchange through the underlying nanofiber mat; and easy integration into standard two-chamber cell culture well systems.

Introduction

Conventional 2D culture systems frequently distort normal cell behavior because they are unable to faithfully recapitulate *in vivo* cell interactions with the surrounding microenvironment. Cell morphology, metabolism, gene and protein expression, differentiation patterns, and intracellular signaling, among other factors, can be greatly altered.[1,2] Many cell types – *e.g.* hepatocytes, pancreatic cells, embryonic stem cells, and cardiomyocytes – exhibit more tissue-like behavior when cultured in 3D aggregates/clusters.[1,3–5] This configuration more closely resembles the *in vivo* environment and therefore favors proper cell physiology. Cell clusters have thus been increasingly used as models in drug development and studies of tumor behavior, tissue morphogenesis, apoptosis, and differentiation.[3,6,7]

Cell aggregates have also been studied for the development and implementation of cell-based therapies. Liver failure is a pertinent example affecting many people worldwide.[8,9] Liver transplantation is currently the only definitive treatment; however, a lack of donors drives other approaches for either partial or total recovery of function. Liver assist devices (LAD) can be used to sustain hepatic functions.[10] Bioartificial liver devices (BAL) are attractive because they could potentially replicate complex biological pathways such as detoxification, hormonal regulation, lipid and glucose metabolism, pH regulation, protein synthesis, and bile production.[10] Growth in the field of hepatic tissue engineering has primarily been focused on the regeneration/replacement of hepatic tissue or the development of functional substitutes such as implantable cellular constructs.[11–15] As envisioned, both BAL systems and tissue engineering approaches will utilize hepatocyte clusters due to their highly functional character and similarity to *in vivo* morphological and functional properties. Moreover, cell viability and functionality are retained for longer periods of time in comparison to traditional monolayer cultures.[16] Studies have also shown that clusters containing hepatocytes and stromal hepatic cells present enhanced long-term functionality.[17] Cell clustering has also shown promise in the development or improvement of cell therapies for the treatment of type I diabetes.[4,5,18]

Many strategies have been developed to induce 3D cell aggregation. These include cultivation in hanging drops, non-adhesive surfaces, shake flasks, gyratory shakers, roller bottles,

[a]*Department of Biomedical Engineering, The Ohio State University, 270 Bevis Hall, 1080 Carmack Rd., Columbus, OH, 43210, USA. E-mail: hansford.4@osu.edu; Fax: +1 614 292 7301; Tel: +1 614 688 3449*
[b]*NSF Nanoscale Science and Engineering Center, The Ohio State University, 1381 Kinnear Rd., Suite 100, Columbus, OH, 43212, USA*
[c]*William G. Lowrie Department of Chemical and Biomolecular Engineering, The Ohio State University, 125 Koffolt Laboratories, 140 West 19th Ave., Columbus, OH, 43210, USA*
[d]*Department of Materials Science and Engineering, The Ohio State University, 477 Watts Hall, 2041 College Rd., Columbus, OH, 43210, USA*
† Electronic supplementary information (ESI) available: Supplementary figures showing micrographs of micro/nanodevices with more complex geometries, fluorescence microscopy images showing cell seeding results with other cell lines and/or seeding methods, and confocal microscopy images of C3A cell cultures on conventional microwell arrays for 4 and 8 days. Supplementary table showing the fabrication parameters of the microwell arrays. See DOI: 10.1039/b919475d
‡ Equal contribution.

and gel encapsulation.[3,19–21] Most of these techniques, however, offer little to no control over cluster size and morphology. This could be problematic, as undefined cluster growth could lead to the formation of necrotic cores due to limited waste/nutrient exchange. Cell behaviors are known to be influenced by geometric factors such as cluster size and morphology,[22,23] and thus these must also be well defined. Approaches like gel encapsulation and gravity-enforced cell assembly typically provide better control over cluster size; however, these methods tend to be laborious, limiting the scale-up necessary for their envisioned usage.

Recently, microfabrication techniques have been applied to develop arrays of microwells to create cell aggregates in a more controlled and efficient manner.[24–29] In these arrays, the cells are allowed to passively settle within the wells *via* sedimentation, and the cells outside the wells are carefully rinsed away. In other cases, the bottom of wells was functionalized with certain molecules that promote preferential cell adhesion.[28] With such systems, microwell size and morphology can define the geometric properties of the aggregate.

In contrast to these systems, we have developed a microwell-based platform in which the well bottom is made entirely of nano/microscale polymer fibers. This is achieved using electrospinning, a versatile technique that can produce nonwoven mats of fibers with essentially any chemistry and diameters ranging from 15 nm to 10 μm.[30,31] The platform consists of a microfabricated array of through-thickness wells firmly interfaced with a sheet of electrospun fibers upon which cell clusters self-assemble within the confines of each microwell. This underlying fibrous bottom confers a number of advantages over previously developed microwell approaches. Such nanofibrous environments have consistently shown to promote more *in vivo*-like cell behavior than standard culture surfaces.[32,33] Previous studies showed that rat hepatocyte clusters present enhanced functionality when cultured on a nanofibrous scaffold.[34] In addition to the advantages of a more *in vivo*-like topography, the porous fiber provides more efficient nutrient delivery and waste removal to a functional cluster, and allows for the application of gentle suction to guide cell loading, if required. Moreover, this platform can be combined with other cell types to potentially make active use of cell–cell signaling to improve functionality. The platform thus has the ability to conduct more biologically relevant studies of key cellular processes. Here we explore the use of this platform to control clustering and function of hepatocytes, of relevance to BAL.

Results

Micro/nanodevice for spatially controlled assembly of cell clusters

Micro- and nanofabrication techniques were combined to develop a platform for applications in high throughput controlled assembly of cell aggregates. Soft lithography micromolding and spin dewetting on a micropatterned poly(dimethylsiloxane) (PDMS) stamp[35] were used to create arrays of through-thickness wells from different polymers (polycaprolactone, PCL, and polystyrene, PS), well geometries (circles, triangles, squares), and dimensions (20–300 μm) (Fig. 1a). For electrospinning, up to 16 arrays (~1.86 cm^2 each) at a time were placed on the collector of the electrospinning apparatus. Polymer fibers (PCL, polyethersulfone (PES), and gelatin) were then electrospun for different time periods, depending on the desired thickness of the fibrous mat. For ~100 μm thick mats, the time ranged from ~10 to 30 min, as determined by the type of polymer and electrospinning conditions. Fiber size varied from the nano- to micrometer range (Fig. 1c–i). PCL and PES fibers presented cylindrical geometry, while gelatin fibers exhibited a ribbon-like structure. Previous studies have attributed this morphology to the formation and subsequent collapse of a skin on the surface of the jet.[30] The small traces of residual solvent left in the fibers immediately after deposition helped to bond the fibrous mat with the polymeric well array (Fig. 1c, inset). Other techniques such as temperature-assisted (Fig. S1†) or CO_2 bonding[36] could also be employed in the assembly of micro/nanodevices when the presence of residual solvent in the fibers is not sufficient to achieve strong adhesion. Conventional microwell arrays (*i.e.* with solid polymer well bottoms) were also fabricated (Fig. 1b) for comparison purposes.

The versatility of our fabrication method allows for the implementation of many materials and fabrication conditions to obtain devices with physical and chemical properties that can meet specific requirements in different applications beyond guided 3D cluster formation. Using a similar fabrication approach we were able to manufacture more complex structures by controllably combining micro- and nanofeatures with different geometries and chemistries. Such structures could be implemented in a number of different applications, including the development of inherently multi-cellular tissue engineering scaffolds. As such, these scaffolds would be more capable of resembling the native tissue environment both in terms of *in vitro* biology through cell–cell signaling and through the morphological control at the micro- and nanoscale to pre-form cellular distributions closer to those found *in vivo* (Fig. S1† shows examples of the morphological control).

Preferential cell seeding inside the microwells

To demonstrate preferential cell seeding inside the microwells we used the patterned arrays of 20, 150, and 300 μm PS microwells bonded to PCL fibers. Human hepatoblastoma C3A cells served as our cell model. A two-step seeding procedure was implemented. The cells were suspended in medium and seeded on the platform at a density of 2.5×10^5 cells cm^{-2}, followed by a ~2 h incubation to allow cell settling. The medium was subsequently removed, and the cells that remained outside the wells were extracted by gently rinsing with phosphate-buffered saline (PBS). The strongly hydrophobic character of native PS (in contrast to that of oxidized tissue culture PS) effectively prevented cell adhesion on the array surface.[37] The limited adhesiveness of the microwell array material, combined with enhanced cell retention on the fibrous regions possibly conferred by the 3D character of the fibers, favored preferential cell seeding inside the fibrous wells (Fig. 2a-20 μm wells, Fig. 2b-150 μm wells) in comparison to conventional wells (Fig. 2c). Alamar blue measurements confirmed improved cell retention on the micro/nanodevice following the PBS rinse (Fig. 2d). Previous reports have postulated that microwells provide shear-protected regions, which

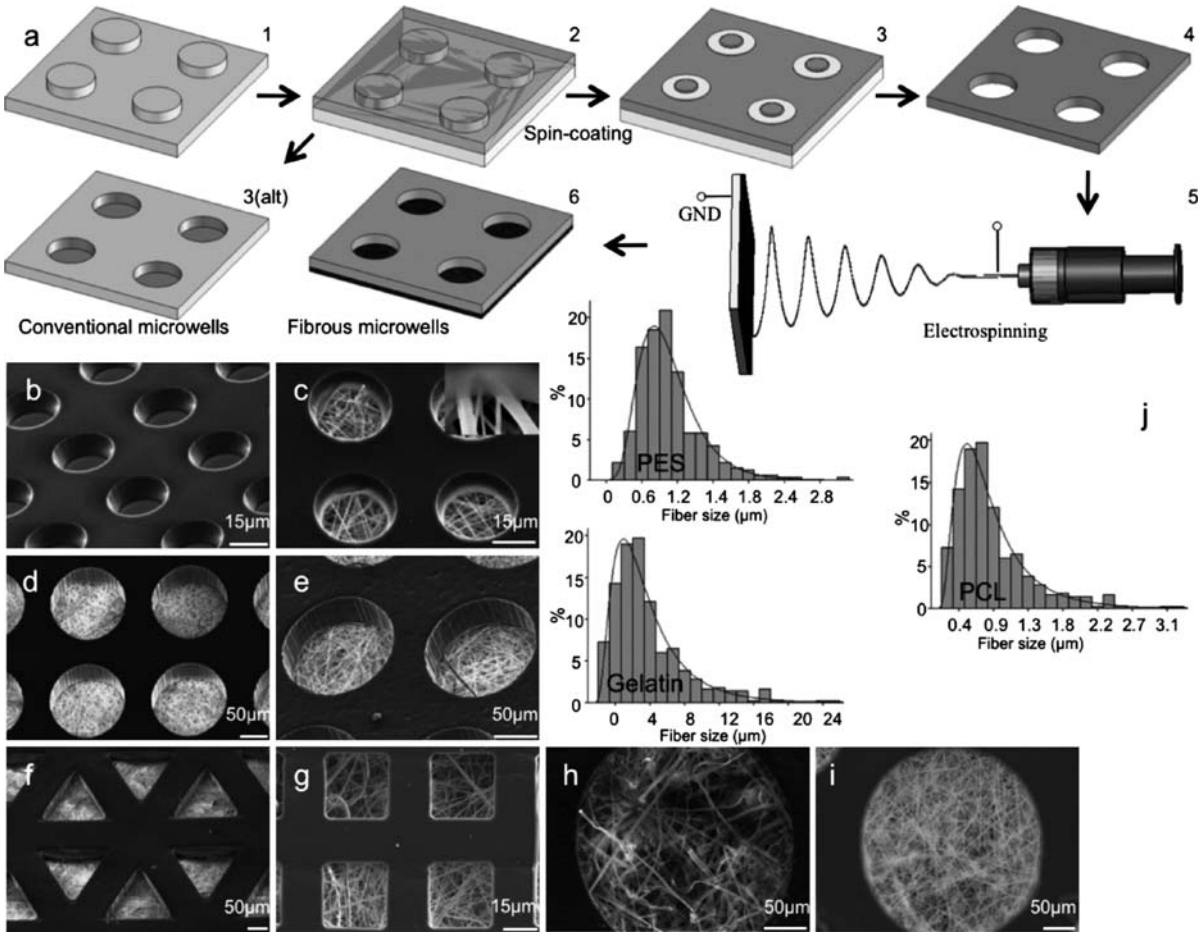

Fig. 1 Fabrication of the micro/nanodevice. (a) Illustration of process: (1) PDMS stamp; (2) drop-cast polymer solution; (3(alt)) solvent is evaporated and the polymer is peeled off to create a conventional microwell array; (3) polymer solution is spin-coated and de-wets on the surface of the PDMS stamp; (4) microwell array is peeled from mold; (5) fibers are electrospun on the microwell array; (6) completed microwell array with fibrous bottom. (b) Conventional PS microwell array (20 μm diameter). (c and d) PS microwells (20 and 150 μm diameter, respectively) bound to PCL fibers. (e–g) PCL microwells (different geometries) bound to PCL fibers. (h and i) PCL microwells bound to gelatin and PES fibers, respectively. (j) Histograms showing fiber size distribution (bars = experimental data, fit = 3-parameter lognormal).

decrease the chances of removing the cells from inside the wells during routine rinses and media changes.[26] While shear protection may increase the cell retention compared to a flat surface, it was not sufficient to retain cells within the conventional microwells fabricated from PS (Fig. 2c). The number of cells per microwell, determined from fluorescence microscopy images of cell-containing wells using image analysis software (UTHSCSA Image Tool), was reasonably well-controlled for defined dimensions of the wells (Fig. 2e).

Other approaches have been investigated to precisely organize cells in clusters using external forces. Albrecht *et al.* used dielectrophoretic forces to form spatially organized cell clusters within a photopolymerizable PEG gel.[38] We were also able to use external forces (*i.e.* vacuum) to trap cells inside the microwells of our platform without having to rely on fiber-mediated cell retention and shear protection. The porous well bottom allowed us to apply suction (10–25 inHg) through the back side of the platform and selectively pull cells from suspension into the wells (Fig. S2†). Preferential cell seeding either *via* active (*i.e.* vacuum-assisted) or passive means (*i.e.* cell settling) was also demonstrated with other cells of interest, including HL1 mouse cardiomyocytes, D3 mouse embryonic stem cells, and PANC-1 pancreatic ductal epithelial-like cells (Fig. S2†).

Formation of hepatocyte clusters on the micro/nanodevice

Devices with PCL microwell arrays (150 and 300 μm diameter) and PCL fibers were used in these experiments. C3A cells were seeded using the conditions described above. Preferential cell seeding was also observed in these devices (Fig. 3). This further supported our hypothesis that this phenomenon was mainly governed by structural and topographical cues presented by the fibrous well bottom and not by the difference in surface chemistry between wells and fibers. Alamar blue measurements immediately after the PBS rinsing step, along with fluorescence/confocal microscopy images, confirmed superior cell retention in comparison to conventional PCL microwell arrays ($p = 0.0001$) (Fig. 3a). The number of cells inside the conventional microwells and the overall degree of organization were considerably reduced, as seen previously with conventional PS microwells. Longer term culture demonstrated that this disordered cell behavior on conventional microwell arrays continued for several days; no

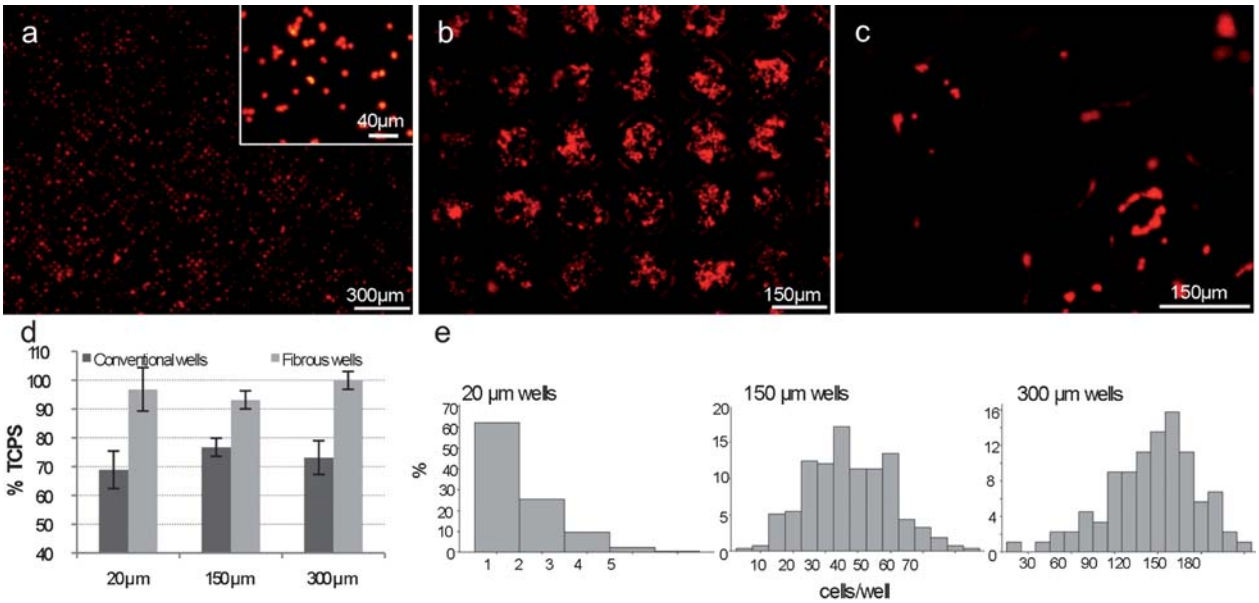

Fig. 2 Preferential cell seeding inside the fibrous microwells (PS wells/PCL fibers). Cell nuclei were stained red with PI-RNase. (a) C3A cells seeded inside 20 μm wells, (inset) magnified view of cells in individual wells. (b) C3A cells seeded inside 150 μm wells. (c) C3A cells seeded on a conventional PS microwell (150 μm diameter) array. (d) Alamar blue results confirming increased metabolic activity/retention on the device with fibrous wells in comparison to conventional microwells. (e) Histograms of the number of cells per well on fibrous wells (*x*-axis units are "number of cells per well").

signs of recovery (Fig. S3†) were noted. Therefore, cluster formation and progression were only monitored on wells with fibrous bottoms, and compared to tissue culture polystyrene (TCPS). Optical, confocal, and scanning electron microscopy (SEM) revealed that C3A cells formed 3D clusters inside the wells after 4 days of culture (Fig. 3d–i). In comparison, C3A cells on TCPS formed a 2D monolayer. To the best of our knowledge there are no previous reports showing hepatocyte cluster formation on pure PCL electrospun fibers. We speculate that PCL fiber hydrophobicity decreased cell adhesion, which enhanced cell–cell interactions and facilitated clustering. Alamar blue was also used to evaluate cellular metabolic activity (*i.e.* oxidation–reduction) in the clusters over a period of 8 days. Metabolic activity was slightly decreased on the platforms with respect to TCPS at $t = 2$ and 4 days (Fig. 3b). Changes in measured metabolic activity reflected combined variations in viability, proliferative and metabolic capacities. A decline in cell viability was ruled out, as confocal microscopy analysis of calcein-stained cells did not show necrotic areas (Fig. 3f and g). We speculate that this difference could possibly be from a delay in hepatocyte proliferative activity, as a result of changes in gene and protein expression (*e.g.* integrins and cadherins) that modulate cell–matrix and cell–cell interactions and ultimately lead to 3D cluster formation.[40,41] Nevertheless, after 8 days of culture, metabolic activity was considerably higher on our device (for both 150 and 300 μm wells) compared to TCPS ($p = 0.0003$). The lower metabolic activity observed on TCPS was attributed to the fact that the cells grew to form a confluent 2D monolayer and possibly suffered from contact inhibition, while the C3A cells on the periphery of the clusters could continue proliferating.[39]

When the increased rate of metabolic activity (with respect to TCPS) was considered (from days 4 to 8), we found a significantly higher ($p = 0.015$) value for platforms utilizing 150 μm wells (12.46 ± 0.61% per day) compared to 300 μm wells (10.27 ± 0.70% per day). Smaller wells tend to favor longer term cell activity, as it is well established that 3D cell clustering, if uncontrolled, could affect cell viability and functionality due to limitations in mass transfer. Oxygen/nutrient supply and waste removal completely depend on diffusion due to the absence of aggregate vascularization. Previous studies have concluded that the maximum spheroid diameter that avoids impaired oxygen transport is ~100 μm.[42]

We investigated hepatocyte-specific functions on our platform after 2, 4 and 8 days of culture by measuring urea synthesis from medium aliquots. The results show enhanced urea synthesis on our platform compared to the cell monolayer on TCPS at all times (Fig. 3c). Urea synthesis rate remained relatively constant, and was higher on 150 μm well devices ($p = 0.01$), compared to 300 μm well devices on day 4. No significant differences were found at or between days 2 and 8. The production of urea was normalized to the number of wells on each device for a given area (~1400 and ~5700 for 300 and 150 μm wells, respectively). The average synthesis rate over 8 days was approximately 13.7 ± 1.7 and 52.06 ± 3.3 ng per day per 10^6 cells per well for devices with 150 and 300 μm wells, respectively. This correlated well with the approximate number of cells per well for each diameter. Overall, the urea production levels were comparable to previous literature reports on C3A cell clustering.[39]

Control of cluster shape and cell co-cultures

The importance of precisely controlling microtissue size and shape has been emphasized by many authors.[24,38,42] The lack of homogeneity in these variables could affect cell functions. Our fabrication approach allows us to create arrays of wells with numerous shapes and sizes by changing the design of the

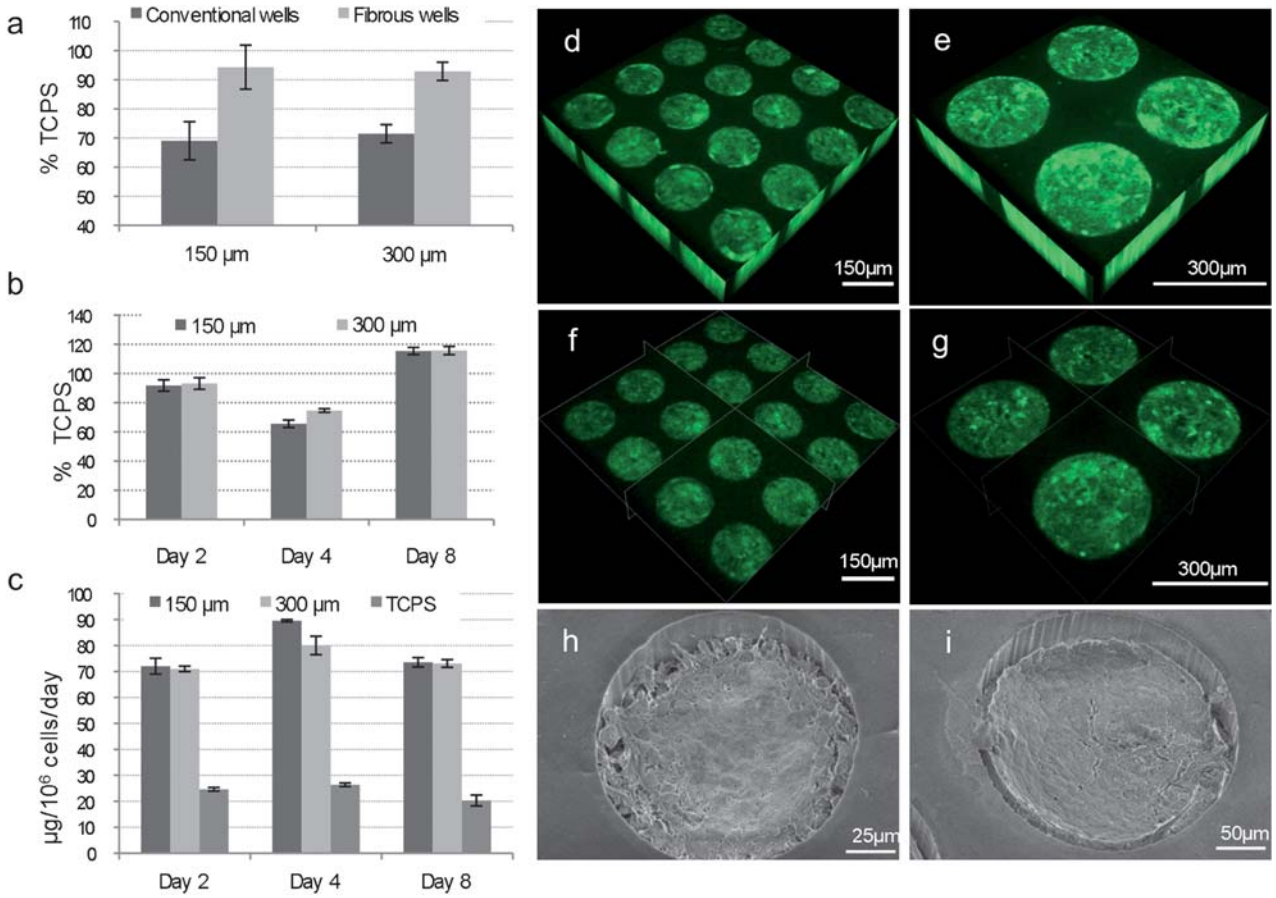

Fig. 3 Guided assembly of hepatocyte clusters (PCL wells/PCL fibers). (a) Alamar blue results showing enhanced cell activity/retention for the fibrous wells. (b) Cellular metabolic activity over 8 days. (c) Urea synthesis rate. (d–g) Confocal microscopy images of hepatocyte clusters on the micro/nanodevice (live cells were stained green with Calcein AM). (d and e) Hepatocyte clusters inside 150 μm (4 day culture) and 300 μm (8 day culture). (f and g) Images of the cross-section of (d) (cluster thickness ~53 μm) and (e) (cluster thickness~66 μm) showing live cells in the center of the clusters. (h and i) SEM micrographs of the clusters inside 150 μm and 300 μm wells, respectively, after 8 days of culture.

patterned PDMS mold. Using the same seeding protocol, we were able to create hepatocyte clusters in wells having a range of different geometries. SEM revealed that the clusters conformed to the geometry of the well (Fig. 4d and e). The ability to control geometric factors could be important in achieving optimal cell functionality. Defining an optimum well geometry, where cell functionality is maximized with respect to others, will require additional studies that factor in the cell type and final application (among other variables), which are beyond the scope of this paper. Moreover, custom-designed microtissues could be used to help develop a better understanding of certain aspects of tissue morphogenesis (and/or other important biological processes), and could also be implemented in a number of cell-based therapy and tissue engineering approaches.

Finally, we demonstrated the ability of our platform to allow the formation of semi-controlled heterotypic cell interactions by co-culturing hepatocytes with NIH 3T3 fibroblasts. Proper tissue development and function generally depend on spatially and temporally controlled heterotypic and homotypic cell interactions. In addition to hepatocyte–hepatocyte interactions, heterotypic interactions with non-parenchymal cells have been shown to stabilize the phenotype of hepatocytes and enhance cell functionality and viability.[43,44] Cell co-cultures have also been utilized in many other studies as a means of improving cellular responses. Different microfabrication-based approaches have been investigated to create organized co-cultures.[45,46] The fibrous well bottom of our platform, besides providing topographical and/or chemical stimulation to the cells, could also be used to enable semi-controlled cell–cell interactions by co-culturing cells on opposite sides of the platform using a two-chamber membrane-based approach (Fig. 4a–c). The physical (*e.g.* thickness, porosity) and chemical (*e.g.* hydrophilicity, functional groups) properties of the fiber mat can be readily modified to regulate the degree of cell–cell interactions. To illustrate this, we seeded the hepatocytes on PCL devices with triangular wells, and the fibroblasts were seeded 24 h later either on the opposite (configuration A) or same side (configuration B) as the hepatocytes. A 1 : 1 hepatocyte : fibroblast ratio was used in both cases. C3A cells cultured alone in the wells were used as control. Urea synthesis was measured and normalized to the control after 7 days of co-culture. SEM was used to visually evaluate the co-cultures. The results show that C3A–3T3 co-cultures were successfully maintained on our platform for up to 7 days. For configuration B we saw that in most cases the fibroblasts invaded the wells and/or grew directly on top of the hepatocyte clusters (Fig. 4g). In configuration A, the fibrous mat provided a physical

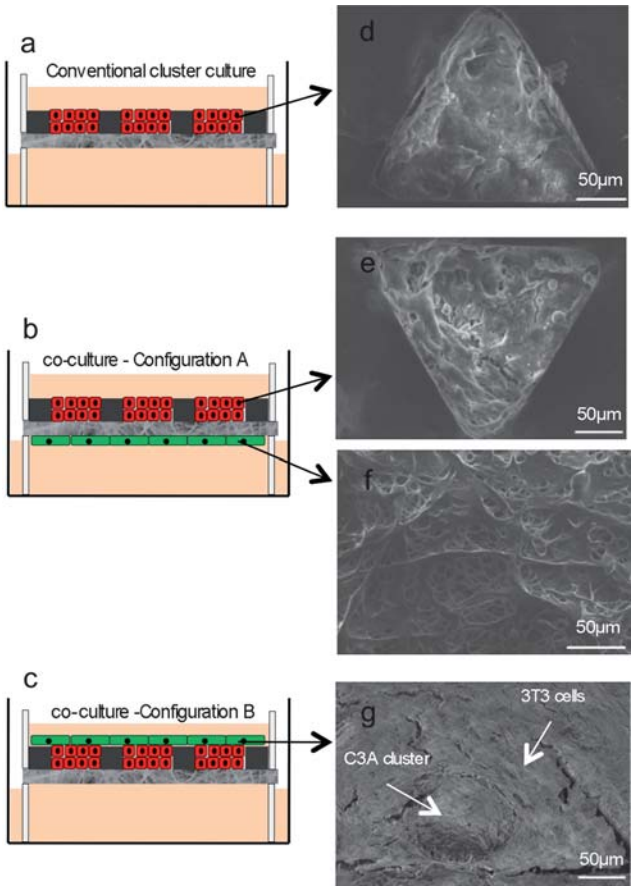

Fig. 4 Clusters with different morphologies and cell co-cultures. (a–c) Different culture/co-culture configurations that can be explored using a two-chamber membrane-based system. (d and e) Hepatocyte clusters in triangular wells conforming to the geometry of the well. (f) 3T3 cells growing on the opposite side to the wells/C3A clusters. (g) C3A–3T3 same side co-cultures (the 3T3 cells appear to be invading the wells and/or growing on top of the C3A clusters).

barrier that prevented cell invasion and cross-contamination (Fig. 4e and f). Cell–cell contacts, if desired, could be permitted by modifying the porosity and sheet thickness. This allows for more controlled studies on cell–cell interactions. A slight enhancement in urea synthesis was detected in these co-cultures. Urea synthesis increased by 4.01 ± 2.38% in configuration B relative to the monoculture control. In comparison, we detected a significantly higher increment in urea synthesis of 10.04 ± 1.81% ($p = 0.02$) for configuration A. The high porosity of the fibers and the chosen thickness of the sheet (~100 μm) facilitated cell communications and favored hepatocyte functions possibly through the release of soluble factors and/or direct cell–cell interactions. The smaller improvement seen in configuration B could be due to the fact that the 3T3 cells had a tendency to invade the wells and grow onto the hepatocyte clusters. This possibly affected proper oxygen diffusion to the cluster and/or urea release from the cluster into the medium. Modifications in the co-culture set up, such as changes in the fiber mat properties, the use of cells that are more reactive/influential in co-culture conditions, and the use of different cell : cell ratios or cell culture conditions (*e.g.* static *vs.* dynamic), could be introduced to further enhance cell function.[43,47,48]

Discussion and conclusions

A platform that supports high throughput assembly of spatially controlled microscale tissue subunits was developed by combining simple and cost-effective micro- and nanofabrication techniques. The fabrication of the device was demonstrated with different polymers of biomedical interest. Hepatocyte clusters were used as a case study; however, preliminary experiments with other cell lines also showed the potential applications of this device in other fields. Our results showed that the fibrous well bottom enhanced cell retention and allowed spatially controlled assembly of cell clusters. The geometrical properties of the wells can be easily modified to obtain microtissues with numerous sizes and shapes. Our work suggests that functional hepatocyte clusters could be formed on pure PCL fibers. However, the fabrication process allows the use of different types of fibers for specific modifications of cellular functions. For example, Chua *et al.*[34] reported enhanced hepatocyte functions on galactosylated fiber mats, possibly due to interactions between the galactose and the ASGPR cell receptor.

The porous nature of the nanofiber mat at the bottom of the well confers a number of advantages over previously developed conventional microwell arrays intended for the same applications. Fiber geometry and chemistry can be engineered to meet specific requirements in different applications. Electrospun fibers tend to more closely resemble the architecture of the extracellular matrix *in vivo*, and could be used to provide topographical and structural cues that favor appropriate cell function. Fiber chemistry could also be altered to impart appropriate chemical stimulation. A number of materials (*e.g.* synthetic and natural polymers, ceramics, and blends) and fiber chemistry modification strategies (*e.g.* wet chemistry, encapsulation, functionalization, incorporation of nanomaterials, core–sheath) could be implemented for this purpose.[30] The porous well bottom provides an open pathway for medium inflow/outflow that facilitates more suitable nutrient-oxygen/waste exchange for better cell viability and functionality. Moreover, as we have demonstrated, the porous well bottom can be used to apply vacuum through the fiber mat and actively drive the cells into the wells to achieve organized cell distribution. Finally, our platform can easily be integrated into a two-chamber membrane-based system, using several configurations, to allow for more insightful studies and applications (*e.g.* co-cultures, transport, polarization, chemotaxis, and secretion). We showed that the fabrication process developed for our micro/nanodevice is compatible with multiple materials and micro/nanostructures. A similar approach could be followed to develop a wide variety of structures that can be implemented in a myriad of different applications.

In summary, we have presented a method to produce more consistent and functional cell clusters using micro/nanodevices that can be fabricated from many different polymers of interest. The potential application of these devices in the field of guided assembly of microscale tissue subunits has been demonstrated using hepatocytes, with discussion of other potential applications. Our platform could potentially be used in high throughput screening of cell clusters (*e.g.* for drug discovery and studies in cellular and developmental biology), or incorporated into numerous cell-based therapy studies and applications.

Materials and methods

Platform fabrication and characterization

Arrays of through-thickness microwells with different geometries, sizes and configurations were fabricated from PS (Aldrich, melt flow index 4.0) and PCL (Aldrich, M_n 80 000) *via* soft lithography. The geometry and size of the structures were first defined on a silicon master using standard UV photolithography. Positive and negative tone photoresists SPR 220-7 (Shipley) and SU-8 2075 (Microchem Corp.), respectively, were used in the fabrication of the masters. The resists were spin-coated on a silicon wafer at different speeds to produce features with different thicknesses. The photoresists were then exposed to ultraviolet light through a photomask with designed feature geometries, and post-processed following the parameters suggested by the manufacturer. The masters were then used to create negative PDMS molds. The patterned stamps were spin-coated with polymer solutions in anisole under appropriate spin speeds and solid contents to obtain films with the desired thicknesses on the PDMS mold. Table S1† shows the fabrication parameters used in each case. The PDMS molds were then placed on a hotplate at 100 °C for 5 min to drive off the residual solvent and anneal the polymer. After cooling, the polymer microwell arrays were manually peeled off and prepared for electrospinning.

The microwell arrays were placed on the collector of the electrospinning apparatus. Polymer fibers having the desired chemistries and morphologies were electrospun on the arrays. Electrospinning conditions (solution concentration, voltage, and extrusion rate) varied for each polymer. PCL (Aldrich, M_w 65 000) fibers were electrospun using a 15% (w/w) solution in anhydrous acetone, 24 kV, and 15.0 ml h^{-1}. For PES (Goodfellow Corp., M_w 55 000), an 8% (w/w) solution in hexafluoroisopropanol (HFIP) was used, at 13 kV, and 2.0 ml h^{-1}. Finally, for gelatin (porcine skin gelatin type A, Sigma), a 7% (w/w) solution in HFIP, 24 kV, and 15 ml h^{-1} were used. Solutions in HFIP were electrospun in a chemical fume hood. The distance between tip and the collector was maintained at 20 cm. Conventional microwell arrays were fabricated by drop-casting the polymer solution on the PDMS stamp, drying out at 125 °C for 20 min, and peeling off after cooling. SEM (Hitachi S-3000H) was used to characterize the platforms. The devices were coated with a thin Au/Pd layer prior to imaging to prevent charging. Fiber sizes were quantified using the SEM micrographs and image analysis software (Image J).

Cell culture

Human hepatoblastoma cells (C3A, ATCC) were regularly maintained in minimum essential medium (MEM, ATCC), supplemented with 10% fetal bovine serum (FBS, ATCC) and 1% of antibiotics : antimycotics mixture (ATCC). NIH 3T3 mouse fibroblasts were expanded in Dulbecco's modified Eagle's medium (DMEM) supplemented with 10% calf serum (CS, ATCC) and 1% antibiotics : antimycotics. All cell lines were incubated in a humid atmosphere at 37 °C and 5% CO_2.

Cell seeding

The platforms were cut into 15 mm diameter circles and affixed to the bottom of 12 well plates using vacuum grease (Dow Corning). The samples were sterilized with 70% ethanol–PBS (ATCC) rinses, and a 30 min exposure to ultraviolet light in a laminar flow hood. The cells were seeded on each platform at a density of 2.5×10^5 cells cm^{-2} in 1.5 ml of medium, and incubated for approximately 2 h. The medium was removed from the plates, and the samples were gently rinsed with PBS to remove unanchored cells. New medium was added to the samples and they were further incubated for the prespecified time periods. Media changes were performed every 2 days.

Cell co-cultures

Co-cultures were performed using a two-chamber membrane-based approach. The platforms were clamped in-between two hollow polypropylene tubes (~12 mm inner diameter). Vacuum grease was used to seal and secure the pieces together. These constructs were then placed in 24-well plates and sterilized by rinsing with 70% ethanol and PBS, and UV light exposure for 30 min. C3A cells were seeded in the microwells and cultured for 24 h following the procedure described before. NIH 3T3 fibroblasts were then seeded either on the same side as the C3A cells or on the opposite side of the platform after flipping over the constructs. In the later case, the fibroblasts were allowed to attach for several hours (~3 h) before flipping the constructs back over and proceeding with the incubation. Co-cultures were maintained for 7 days. Medium was replaced every 2 days.

Fluorescence, confocal and scanning electron microscopy

For live staining, C3A cells were exposed to calcein green AM (Invitrogen) following the protocol provided by the manufacturer. The nuclei of fixed cells were stained with a PI-RNase solution (BD Biosciences). Cells were fixed in 70% ethanol at −20 °C for 30 min. For SEM imaging, the cells were dehydrated and dried in a series of ethanol solutions (70, 80, 90, and 100%) and hexadimethylsiloxane (HMDS). The samples were then sputter coated with a thin Au/Pd layer.

Measurements of cellular activity

C3A cell metabolic activity was measured using the Alamar blue assay (Invitrogen) following the procedure suggested by the manufacturer. Urea synthesis by the C3A cells was measured from medium aliquots using a blood urea nitrogen kit (BUN, Bioassay Systems) following the protocol suggested by the manufacturer.

Statistical analysis

A total of 3 specimens per type of sample were used in the experiments. An ANOVA test with a 95% level of confidence was implemented to detect significant differences.

Acknowledgements

The authors would like to thank the staff of the Ohio Nanotech West Laboratory for technical assistance and Orin Hemminger for assistance with confocal microscopy. Mouse embryonic stem cells and cardiomyocytes were a kind donation from Dr Serge Karpinski (DHLRI, The Ohio State University) and Professor Claycomb (Health Science Center, Louisiana State University),

respectively. This work was supported with funds from AFOSR MURI (Contract No. F49620-03-1-0421), the National Science Foundation (Grant No. EEC-0425626), and the Global Cardiovascular Innovation Center (Cleveland, OH).

References

1 W. Muller-Klieser, *Am. J. Physiol.: Cell Physiol.*, 1997, **273**, 1109–1123.
2 L. A. Kunz-Schughart, K. Kreutz and R. Knuechel, *Int. J. Exp. Pathol.*, 1998, **79**, 1–23.
3 J. M. Kelm and M. Fussenegger, *Trends Biotechnol.*, 2004, **22**, 195–202.
4 M. I. Boretti and K. J. Gooch, *Tissue Eng.*, 2006, **12**, 939–948.
5 M. I. Boretti and K. J. Gooch, *Tissue Eng., Part A*, 2008, **14**, 1927–1937.
6 B. Desoize, *Crit. Rev. Oncol. Hematol.*, 2000, **36**, 59–60.
7 R. C. Bates, N. S. Edwards and J. D. Yates, *Crit. Rev. Oncol. Hematol.*, 2000, **36**, 61–74.
8 T. Rahman and H. Hodgson, *Intensive Care Med.*, 2001, **27**, 467–476.
9 C. Selden and H. Hodgson, *Transpl. Immunol.*, 2004, **12**, 273–288.
10 S. Diekmann, A. Bader and S. Schmitmeier, *Cytotechnology*, 2006, **50**, 163–179.
11 J. W. Allen and S. N. Bhatia, *Semin. Cell Dev. Biol.*, 2002, **13**, 447–454.
12 K. M. Kulig and J. P. Vacanti, *Transpl. Immunol.*, 2004, **12**, 303–310.
13 K. Ohashi, T. Yokoyama, M. Yamato, H. Kuge, H. Kanehiro, M. Tsutsumi, T. Amanuma, H. Iwata, J. Yang, T. Okano and Y. Nakajima, *Nat. Med. (N. Y.)*, 2007, **13**, 880–885.
14 V. L. Tsang, A. A. Chen, L. M. Cho, K. D. Jadin, R. L. Sah, S. DeLong, J. L. West and S. N. Bhatia, *FASEB J.*, 2007, **21**, 790–801.
15 H. C. Fiegel, P. M. Kaufmann, H. Bruns, D. Kluth, R. E. Horch, J. P. Vacanti and U. Kneser, *J. Cell. Mol. Med.*, 2008, **12**, 56–66.
16 J. Z. Tong, S. Sarrazin, D. Cassio, F. Gauthier and F. Alvarez, *Biol. Cell*, 1994, **81**, 77–81.
17 K. Yamada, M. Kamihira and S. Iijima, *Biochem. Eng. J.*, 2001, **8**, 135–143.
18 B. Davani, *Stem Cell*, 2007, **25**, 3215–3222.
19 H. Okubo, M. Matsushita, H. Kamachi, T. Kawai, M. Takahashi, T. Fujimoto, K. Nishikawa and S. Todo, *Artif. Organs*, 2002, **26**, 497–505.
20 V. I. Khaoustov, G. J. Darlington, H. E. Soriano, B. Krishnan, D. Risin, N. R. Pellis and B. Yoffe, *In vitro Cell Dev. Biol.: Anim.*, 1999, **35**, 501–509.
21 M. Khalil, A. Shariat-Panahi, R. Tootle, T. Ryder, P. McCloskey, E. Roberts, H. Hodgson and C. Selden, *J. Hepatol.*, 2001, **297**, 68–77.
22 E. Eschbach, S. S. Chatterjee, M. Nöldner, E. Gottwald, H. Dertinger, K. F. Weibezahn and G. Knedlitschek, *J. Cell. Biochem.*, 2005, **95**, 243–255.
23 R. Clicklis, J. C. Merchuk and S. Cohen, *Biotechnol. Bioeng.*, 2004, **86**, 672–680.
24 J. M. Karp, J. Yeh, G. Eng, J. Fukuda, J. Blumling, K. Y. Suh, J. Cheng, A. Mahdavi, J. Borenstein, R. Langer and A. Khademhossein, *Lab Chip*, 2007, **7**, 786–794.
25 D. H. Kim, J. Park, K. Y. Suh, P. Kim, S. K. Choi, S. Ryu, S. Park, S. H. Lee and B. Kim, *Sens. Actuators, B*, 2006, **117**, 391–400.
26 H. C. Moeller, M. K. Mian, S. Shrivastava, B. G. Chung and A. Khademhosseini, *Biomaterials*, 2008, **29**, 752–763.
27 A. Khademhosseini, R. Langer, J. Borenstein and J. P. Vacanti, *Proc. Natl. Acad. Sci. U. S. A.*, 2006, **103**, 2480–2487.
28 J. Fukuda, Y. Saki and K. Nakazawa, *Biomaterials*, 2006, **27**, 1061–1070.
29 J. Fukuda, A. Khademhosseini, Y. Yeo, X. Yang, J. Yeh, G. Eng, J. Blumling, C. F. Wang, D. S. Kohane and R. Langer, *Biomaterials*, 2006, **27**, 5259–5267.
30 D. Li and Y. Xia, *Adv. Mater. (Weinheim, Ger.)*, 2004, **16**, 1151–1170.
31 J. Lannutti, D. Reneker, T. Ma, D. Tomasko and D. Farson, *Mater. Sci. Eng., C*, 2007, **27**, 504–509.
32 M. Schindler, L. Ahmed, J. Kamal, A. Nur-E-Kamal, T. H. Grafe, H. Y. Chung and S. Meiners, *Biomaterials*, 2005, **26**, 5624–5631.
33 J. T. Fassett, D. Tobolt, C. J. Nelsen, J. H. Albrecht and L. K. Hansen, *J. Biol. Chem.*, 2003, **278**, 31691–31700.
34 K. N. Chua, W. S. Lim, P. Zhang, H. Lu, J. Wen, S. Ramakrishna, K. W. Leong and H. Q. Mao, *Biomaterials*, 2005, **26**, 2537–2547.
35 N. Ferrell and D. Hansford, *Macromol. Rapid Commun.*, 2007, **28**, 966–971.
36 Y. Yang, Y. C. Zeng and L. J. Lee, *Adv. Mater. (Weinheim, Ger.)*, 2004, **16**, 560–564.
37 A. S. Curtis, J. V. Forrester, C. McInnes and F. Lawrie, *J. Cell Biol.*, 1983, **97**, 1500–1506.
38 D. R. Albrecht, G. H. Underhil, T. B. Wassermann, R. L. Sah and S. N. Bhatia, *Nat. Methods*, 2006, **3**, 369–375.
39 T. Elkayam, S. Amitay-Shaprut, M. Dvir-Ginzberg, T. Harel and S. Cohen, *Tissue Eng.*, 2006, **12**, 1357–1368.
40 L. Ruei-Zeng and C. Li-Fang, *Cell Tissue Res.*, 2006, **324**, 411–422.
41 A. Zimmerman, *Med. Sci. Monit.*, 2002, **8**, 53–63.
42 R. Glicklis, J. C. Merchink and S. Cohen, *Biotechnol. Bioeng.*, 2004, **86**, 672–680.
43 S. N. Bhatia, U. J. Balis, M. L. Yarmush and M. Toner, *FASEB J.*, 1999, **13**, 1883–1900.
44 C. Guguen-Guillouzo, B. Clément, G. Baffet, C. Beaumont, E. Morel-Chany, D. Glaise and A. Guillouzo, *Exp. Cell Res.*, 1983, **143**, 47–54.
45 E. E. Hui and S. N. Bhatia, *Proc. Natl. Acad. Sci. U. S. A.*, 2007, **104**, 5722–5726.
46 G. M. Whitesides, E. Ostuni, T. Shuichi, X. Jiang and D. E. Ingber, *Annu. Rev. Biomed. Eng.*, 2001, **3**, 335–373.
47 J. Park, F. Berthiaume, M. Toner, M. L. Yarmush and A. W. Tilles, *Biotechnol. Bioeng.*, 2005, **90**, 632–644.
48 A. P. Leonov, J. Zheng, J. D. Clogston, S. T. Stern, A. K. Patri and A. Wei, *ACS Nano*, 2008, **2**, 2481–2488.

